Z. Phys. C 65, 207–213 (1995)

ZEITSCHRIFT
FÜR PHYSIK C
© Springer-Verlag 1995

Two–proton correlations in the target fragmentation region of nuclear collisions at 200 *A* GeV

WA80 Collaboration

T.C. Awes[5], C. Barlag[4], F. Berger[4], M.A. Bloomer[2], C. Blume[4], D. Bock[4], R. Bock[1], E.-M. Bohne[4], D. Bucher[4], A. Claussen[4], G. Clewing[4], L. Dragon[4], A. Eklund[3], S. Garpman[3], R. Glasow[4], H. Gustafsson[3], H.H. Gutbrod[1], G. Hölker[4], J. Idh[3], P. Jacobs[2], K.H. Kampert[4], B.W. Kolb[1], H. Löhner[6], I. Lund[6], F.E. Obenshain[5], A. Oskarsson[3], I. Otterlund[3], T. Peitzmann[4], F. Plasil[5], A.M. Poskanzer[2], M. Purschke[1], B. Roters[1], S. Saini[5], R. Santo[4], H.R. Schmidt[1], S.P. Sørensen[5,7], K. Steffens[4], P. Steinhaeuser[1], E. Stenlund[3], D. Stüken[4], G.R. Young[5]

[1] Gesellschaft für Schwerionenforschung, D-64220 Darmstadt, Germany
[2] Lawrence Berkeley Laboratory, Berkeley, CA 94720, USA
[3] University of Lund, S-22362 Lund, Sweden
[4] University of Münster, D-48149 Münster, Germany
[5] Oak Ridge National Laboratory, Oak Ridge, TN 37831, USA
[6] KVI, University of Groningen, NL-9747 AA Groningen, Netherlands
[7] University of Tennessee, Knoxville, TN 37996, USA

Received: 13 July 1994

Abstract. Correlations between protons are studied in the target fragmentation region of reactions of protons and ^{16}O with C, Cu, Ag, Au and of ^{32}S with Al and Au at 200 *A* GeV. The emitted protons were measured with the Plastic Ball detector in the WA80 experiment at the CERN SPS. The comparison of the correlation function with calculations, assuming a spherical, gaussian shaped source with a lifetime $\tau = 0$ fm/*c*, allows the extraction of radius parameters. The values are very close to those expected from the geometry of the target nuclei and increase with the target mass as $\propto A_{\mathrm{Target}}^{1/3}$. Even in proton induced reactions the whole target nucleus is involved. The dependence of the radii on centrality, polar angle θ_{lab}, and energy, and their relation to measured proton yields are presented.

1 Introduction

The investigation of the target fragmentation region offers an opportunity to study the interaction of particles emitted from the primary interaction zone with the surrounding nuclear environment (spectator matter). This has been the topic of several earlier WA80 publications [1, 2, 3, 4, 5]. They show that the entire target nucleus is involved in the reaction due to rescattering.

The actual size of the target region, which is participating in the reaction, can be obtained with the help of two-proton correlations, which provide information about the space-time characteristics of the proton source. The shape of the correlation function is dominated by three effects. On the one hand, the long range Coulomb repulsion and the Pauli exclusion between two protons cause an anticorrelation at small relative momenta. On the other hand, the attractive S-wave nuclear interaction gives rise to a maximum in the correlation function at a relative momentum $\mathbf{q} = \mathbf{p_1} - \mathbf{p_2} \approx 40$ MeV/*c*, when the protons are less than about 10 fm apart at the time of emission [6, 7, 8]. The height of this maximum is inversely proportional to the volume of the source and thereby provides means to measure its size. An expression for the two-proton correlation function is given in [7] as,

$$C(\mathbf{P}, \mathbf{q}) = \int d^3r \, F_{\mathbf{P}}(\mathbf{r}) \, |\Phi(\mathbf{q}, \mathbf{r})|^2$$

where $\mathbf{r} = \mathbf{r_1} - \mathbf{r_2}$ is the relative coordinate, $\mathbf{P} = \mathbf{p_1} + \mathbf{p_2}$ is the total momentum and $\Phi(\mathbf{q}, \mathbf{r})$ is the relative wave function of the proton pair. The function $F_{\mathbf{P}}(\mathbf{r})$ contains the phase space distribution of the emitted protons after many-body interactions have ceased.

2 Data analysis

The data were taken with the Plastic Ball detector in the WA80 experimental setup at the CERN SPS. This detector has already been employed in an analysis of two-proton correlations for the reactions Ca + Ca and Nb + Nb at 400 *A* MeV, measured at the Bevalac [9]. The Plastic Ball [10] consists of 655 ΔE-E scintillator telescopes and covers the polar range of $30° \leq \theta_{\mathrm{lab}} \leq 160°$ (which corresponds to the pseudorapidity range $-1.7 < \eta < 1.3$). It allows the identification and energy measurement of positive pions and charged fragments up to helium isotopes.

In ultra-relativistic heavy ion reactions one must cope with very high particle multiplicities. The charged particle density $\mathrm{d}N/\mathrm{d}\eta$ at $\eta = 1$ reaches values of up to 100 for ^{32}S + Au collisions [3]. Obviously, the high multiplicity of particles provides a very difficult enviroment for the Plastic Ball detector. Such a situation approaches the detector limits imposed by the finite granularity. Nevertheless, a sufficiently clean particle identification could be achieved as

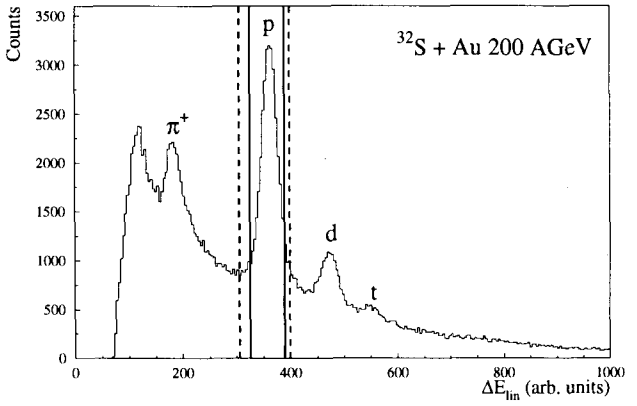

Fig. 1. The linearized ΔE-distribution for the reaction ^{32}S + Au without energy cuts. The ΔE-E bands were linearized and projected onto the ΔE axis. The solid lines mark the identification window used for the ^{16}O- and ^{32}S-induced reactions. The window for data from p-induced reactions is represented by the dashed lines (see text)

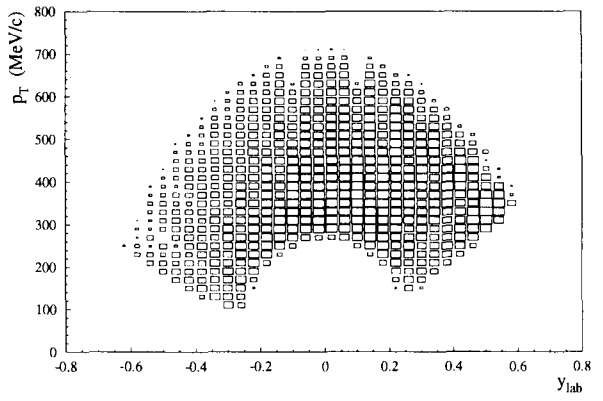

Fig. 2. Phase space density of the accepted protons (log. scale) as a function of p_T and y_{lab} for ^{16}O + Au collisions

demonstrated in Fig. 1 where the linearized ΔE distributions, showing the π^+, p, d and t peaks measured in ^{32}S + Au reactions, are displayed. In order to assure a similar quality of proton identification as is obtained in proton induced reactions, the accepted ΔE-E-band for protons was chosen narrower in the case of ^{16}O and ^{32}S induced reactions. The accepted proton regions are indicated by lines in Fig. 1. In this analysis the energy of the protons is restricted to 40 MeV $\leq E_{kin} \leq$ 200 MeV. This assures that only protons, which are fully stopped in the E-counter and therefore provide a complete ΔE-E-signal, are accepted. Additionally, the misidentification of punch-through deuterons as protons is negligible below the energy limit of 200 MeV. This leads to an acceptance limited in rapidity to $|y_{lab}| \leq 0.6$ and in transverse momentum to 100 MeV/$c \leq p_T \leq$ 650 MeV/c as displayed in Fig. 2.

The WA80 minimum bias trigger requires a valid beam particle in the start counters and at least one charged particle in the multiplicity detectors for all projectile types. For the ion-induced reactions an additional condition demands less then 88 % of the beam energy to be measured in the Zero-Degree-Calorimeter [11] ($\eta \geq 6$). The requirement to

Table 1. Definition of centrality via E_{ZDC}/E_{Beam} together with the average number of target participants $< N_{Part} >$ and the average impact parameter $< b >$ for the Au-target

Centrality	E_{ZDC}/E_{Beam}	$< N_{Part} >$ ^{16}O	$< N_{Part} >$ ^{32}S	$< b >$ (fm) ^{16}O	$< b >$ (fm) ^{32}S
central	0-30 %	38.9	63.8	3.7	3.7
semi-central	30-50 %	23.3	39.9	5.8	5.5
peripheral	50-88 %	9.7	16.9	7.5	7.7

measure at least two protons in the Plastic Ball introduces an additional bias towards more central events. The ZDC is also used for a classification of the events into 3 centrality bins by applying cuts in the measured ZDC-energy. We used the event-generator FRITIOF [12] to extract the average number of target participants $< N_{Part} >$ and the average impact parameter $< b >$ as a measure of the centrality. These variables, which are mainly determined by the reaction geometry, are well described by event-generators like FRITIOF. The values are listed in Table 1 together with the definition of the centrality bins.

The experimental two-proton correlation function is obtained by dividing the distribution of proton-pairs by uncorrelated pairs. The uncorrelated pair distributions were generated with the event-mixing method. To ensure that only protons from comparable events were mixed, the events were divided into 7 classes of centrality and each event was combined with 5 other events of the same event class. Mixed-event pairs with both protons in the same module were rejected. This corresponds to a cut in the opening angle at Ψ = 7°. The correlation function was measured as a function of the Lorentz-invariant relative momentum $Q \equiv \sqrt{-(p_1^\mu - p_2^\mu)^2}$. The resolution in this variable, which is dominated by the granularity of the detector, has an average value of $\sigma_Q \approx$ 23 MeV.

Since there is no simple analytical expression for the two-proton correlation function, which can be fitted to the experimental value, one has to extract the radius parameter R by comparing a numerical calculation to the data. This has been done using a program, which calculates the two-proton correlation function from an assumed phase space distribution of the protons. From this distribution proton pairs are randomly chosen and the square of the relative wave function is calculated, including the effects of the Coloumb repulsion, the Pauli exclusion, and the strong interaction between the proton pairs. Our simulation is based on a spherical, gaussian shaped source distribution ρ with a lifetime of τ = 0 fm/c.

$$\rho(\mathbf{r}, t) = \rho_0 \, exp\left\{-\frac{\mathbf{r}^2}{R^2}\right\} \delta(t - t_0)$$

In the case of a non-zero lifetime this gives an upper limit for the spatial extent of the source. The momenta of the protons were generated according to the measured single-particle distributions.

The original computer code was modified in order to include detector effects [13]. Mainly the angular resolution, limited by the modular structure of the detector, had to be taken into account. Additionally, the energy resolution according to the value measured in [10] was implemented.

Another important point is the possible misidentification of particles in the detector. Protons falsely assigned to other

Table 2. Summary of all analyzed systems with the number of accumulated proton pairs N_{pairs} and the average proton multiplicity $< N_p >$. The values for $< N_p >$ are weighted with the number of proton pairs in each event and efficiency corrected as explained in the text. Also given are the percentages of misidentified particles and the resulting correction factors, which are applied to the result of the simulated correlation function

Reaction	$N_{\text{pairs}} 10^{-3}$	$< N_p >$	Background %	Correction Factor
p + C	58	3.3	10.6 ± 1.1	0.80 ± 0.05
p + Cu	663	5.4	10.1 ± 0.6	0.81 ± 0.05
p + Ag	1318	7.3	10.4 ± 0.4	0.80 ± 0.05
p + Au	4219	10.1	12.4 ± 0.4	0.77 ± 0.05
^{16}O + C	116	3.5	8.8 ± 0.4	0.83 ± 0.05
^{16}O + Cu	1760	7.3	9.5 ± 0.2	0.82 ± 0.05
^{16}O + Ag	4036	11.6	9.8 ± 0.2	0.81 ± 0.05
^{16}O + Au	27316	19.2	12.0 ± 0.2	0.78 ± 0.05
^{32}S + Al	997	4.0	14.0 ± 0.3	0.74 ± 0.05
^{32}S + Au	26696	18.7	14.6 ± 0.3	0.73 ± 0.05

particles are not relevant for this analysis. Particles, that are wrongly accepted as protons, however may influence the correlation function. Reasons for misidentification are :

- The particle is scattered out from the original module into an adjacent module and therefore shows only an incomplete E-signal.
- Deuterons and tritons suffering reaction losses in the scintillator may fall into the proton window.
- Because of the high multiplicity double hits in a module may occur.

The last point is strongly dependent on the hit multiplicity and on the θ_{lab}-angle. The apparent momentum of fake protons bears almost no information on the true momentum of these particles – they are uncorrelated and will reduce the height of the measured correlation function and thereby simulate a larger source. Therefore a correction factor has to be applied to the result of the simulation. To obtain this correction factor, the background of misidentified particles has to be estimated. This was done by fitting a projection of the ΔE-E band of the protons (Fig. 1) with the sum of a Gaussian curve and a polynomial for the background. From the integrals of Gaussian curve plus polynomial and of the polynomial alone in the range of the accepted protons the percentage of misidentified particles is obtained. Because the background is strongly dependent on the multiplicity of the reaction and on the θ_{lab}-range, it is measured for every analyzed system separately. Typical values are given in Table 2. The background for the p- and ^{16}O-induced reactions is, despite the strongly different multiplicity, the same, because the particle identification is less restrictive for the p-projectiles. This table also contains the number of used proton pairs N_{pairs} and the average proton multiplicity $< N_p >$, which is measured with the same proton identification window for the proton- and the ^{16}O- and ^{32}S-data, in order to make a direct comparison possible. The values listed here for $< N_p >$ are weighted with the number of proton pairs in each event and corrected with an efficiency, which was calculated in [1] with a Monte-Carlo method for the reactions ^{16}O + Cu, Ag, and Au. The extracted efficiency corrections are extrapolated for the other reactions. Corresponding to [1] the uncertainty in $< N_p >$ is assumed to be ±15%.

Table 3. Radius parameters R in fm for all analyzed reactions

	Target				
Projectile	Au	Ag	Cu	Al	C
p	3.9 ± 0.24	3.4 ± 0.24	2.7 ± 0.24		1.8 ± 0.24
^{16}O	4.4 ± 0.30	3.8 ± 0.24	3.3 ± 0.24		2.2 ± 0.24
^{32}S	4.2 ± 0.34			2.7 ± 0.24	

The result of the correlation calculation is normalized in the same region as the experimental correlation function: 195 MeV $\leq Q \leq$ 300 MeV. To extract a radius parameter, the calculation is performed for a set of different radius parameters and then compared to the data by calculating the χ^2-value.

The systematic uncertainties are mainly introduced by the imperfect knowledge of the background, caused by the false particle identification. Especially multiple hits of $\pi^{\pm}$, δ-rays, neutrons, and γ's can lead to a signal, which lies in the proton identification window. The relative uncertainty of the correction factor is estimated to be less then 7%. This leads to a variation of the radius parameters of ≤ 0.1 fm. The comparison of two correlation functions measured with different identification windows provides a test for the quality of the background correction. For the reaction ^{16}O + Au this yields a difference in the resulting radius parameters of only 0.1 fm, which is within the range of estimated uncertainty.

The effect of multiple hits also worsens the energy resolution in a way that is not implemented in the simulation. This becomes evident by the fact that the experimental correlation function is not so well reproduced in systems with high multiplicities such as ^{32}S + Au. To estimate the resulting uncertainty, the simulation was artificially adapted to the data by varying the energy resolution parameter in the simulation. This leads to a deviation of the radius parameters by 0.1 fm for ^{16}O + Au and by 0.2 fm for ^{32}S + Au. Bin size effects introduce a further uncertainty of ≤ 0.1 fm.

The total systematic uncertainty is given by the quadratic sum of all of the contributions listed above.

3 Results

Figure 3 shows the two-proton correlations as a function of Q for reactions of 200 GeV protons, ^{16}O, and ^{32}S with different targets. For small values of Q one can see a clear enhancement in the data, corresponding to the two-proton S-wave correlation. The hatched band displays the result of the calculations which gives the best fit to the data. The width of the band represents the uncertainty of the Monte Carlo calculation. Theoretically, one would expect the correlation function to drop to zero for Q = 0 MeV. This value is not reached because of the relative momentum resolution of the detector. However the difference in height of the peak is clearly visible, which corresponds to different underlying source sizes. The extracted radius parameters R are listed in Table 3 for all analyzed systems. These values are also compiled in Fig. 4 where all radius parameters are displayed as a function of $A_{\text{Target}}^{1/3}$. For all projectiles a significant proportionality to $A_{\text{Target}}^{1/3}$ is observed. In the case of the p-induced reactions the radius parameters happen to lie closely below the geometrical nuclear radii, represented by the hatched

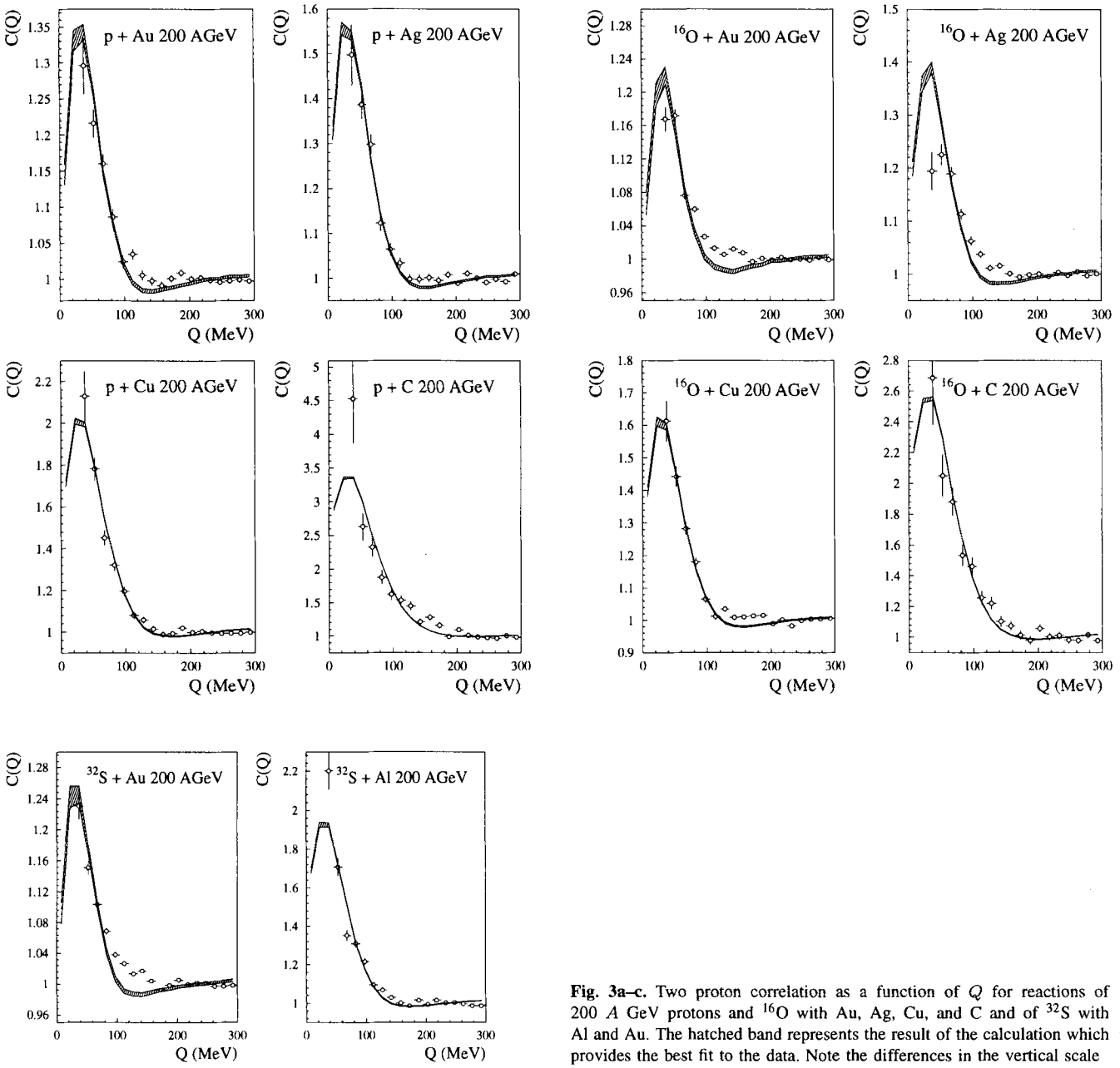

Fig. 3a–c. Two proton correlation as a function of Q for reactions of 200 A GeV protons and ^{16}O with Au, Ag, Cu, and C and of ^{32}S with Al and Au. The hatched band represents the result of the calculation which provides the best fit to the data. Note the differences in the vertical scale

band, while for the ^{16}O and ^{32}S projectiles slightly higher values are found. The rms nuclear radius is here converted into the corresponding Gaussian radius parameters [14]:

$$R_{\text{geo}} = \frac{1}{\sqrt{2}}\sqrt{\frac{2}{3}}\, 1.29\, A_{\text{Target}}^{1/3}$$

A comparison between the p and the ^{16}O-results is attempted by applying a function $R = \alpha A_{\text{Target}}^{\beta}$ to the data for fitting the radius parameters of different target-projectile combinations. The results of this global fit are given in Table 4. For the p-induced reactions there is an indication that the exponent β is slightly greater than for the ^{16}O-reactions, suggesting that the dependence on the target mass is stronger in the proton case.

To investigate the target dependence in more detail, two proton correlations have been studied as a function of the proton emission angle θ_{lab}, the measured proton multiplicity $< N_{\text{p}} >$, the number of target participants N_{Part}, and the center-of-mass energy of the proton pairs E_{cm}.

Protons, which were detected in the forward half ($30° < \theta_{\text{lab}} < 90°$), and those, which hit the backward half ($90° < \theta_{\text{lab}} < 160°$) of the detector, were analyzed separately. The resulting radius parameters are displayed in Fig. 5 again as a function of $A_{\text{Target}}^{1/3}$. The results of the fit with $\alpha A_{\text{Target}}^{\beta}$ are also listed in Table 4. There is an indication that the target dependence is stronger for $\theta_{\text{lab}} > 90°$ than for $\theta_{\text{lab}} < 90°$ with a difference which is larger for the p-induced reactions than for the ^{16}O-induced reactions. For collisions of protons with light targets the absolute values of the radii are significantly larger in the forward hemisphere.

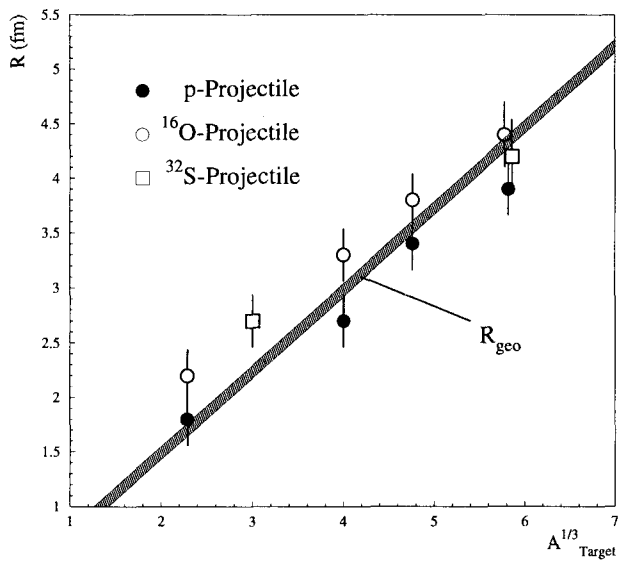

Fig. 4. Target dependence of the radius parameters R for all analyzed reactions with different projectiles. R_{geo} is the geometrical radius of the target nuclei, as explained in the text. The symbols are slightly displaced for the Au-target for clarity

Table 4. The parameters α and β of the function $R = \alpha\, A^{\beta}_{\text{Target}}$ fitting the radius parameters for the p and ^{16}O reactions. Global results for all angles are compared to results for different angular regions

		θ_{lab}-Range		
Projectile	Parameter	Global	$< 90°$	$> 90°$
p	α	0.8 ± 0.3	1.0 ± 0.5	0.4 ± 0.3
	β	0.29 ± 0.08	0.26 ± 0.10	0.41 ± 0.17
^{16}O	α	1.2 ± 0.3	1.3 ± 0.3	0.8 ± 0.4
	β	0.25 ± 0.06	0.22 ± 0.05	0.35 ± 0.12

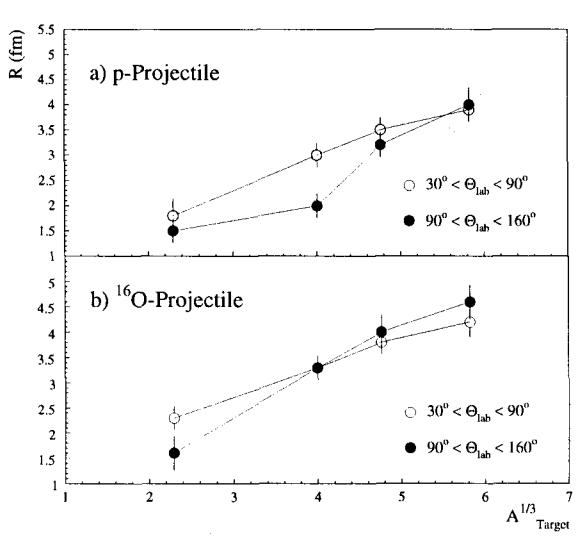

Fig. 5. Target dependence of the radius parameters R for p- and ^{16}O-induced reactions in the forward ($30° < \theta_{lab} < 90°$) and the backward ($90° < \theta_{lab} < 160°$) hemisphere of the detector. The lines are displayed in order to guide the eyes

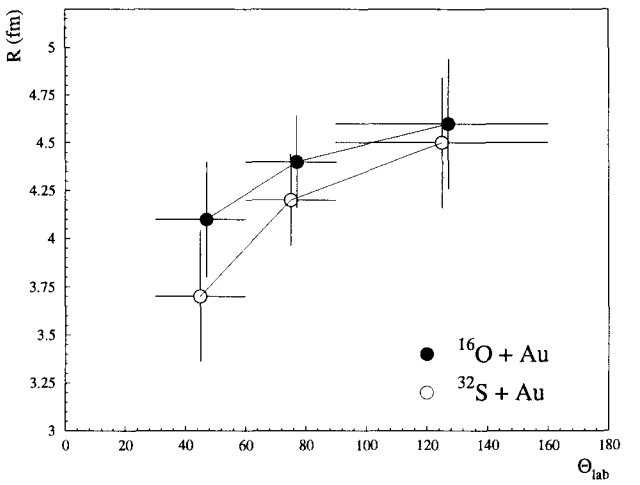

Fig. 6. Radius parameters R as a function of the polar angle θ_{lab} for ^{16}O and ^{32}S + Au collisions. The symbols are slightly displaced for clarity

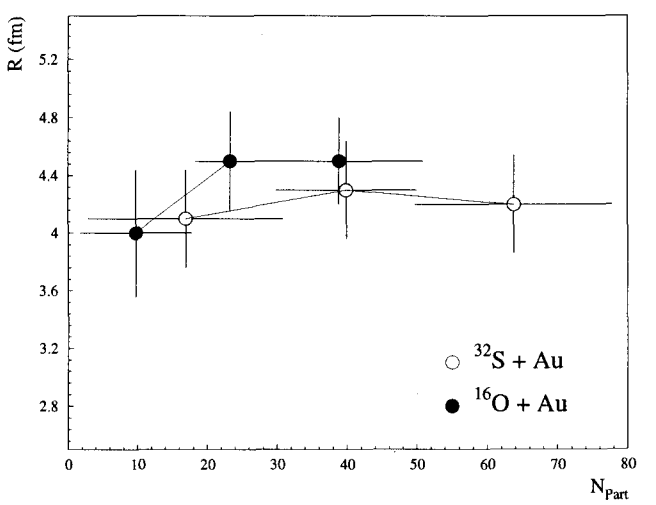

Fig. 7. Radius parameters R for ^{16}O and ^{32}S + Au reactions as a function of the number of target participants N_{Part}

A more detailed view of the θ_{lab} dependence for ^{16}O and ^{32}S + Au is given in Fig. 6. In the case of the ^{32}S-induced reactions a significant rise of the radius parameters with θ_{lab} is visible. The same effect shows up for ^{16}O + Au, but is less pronounced.

To study the centrality dependence of the radius parameters, the analysis was performed for ^{16}O- and ^{32}S-collisions in three different E_{ZDC}-regions. The results are displayed in Fig. 7 as a function of the number of target participants (see Table 1), to make a direct comparison between the two systems possible. Only a small variation over this large range of N_{part} is observable, even for peripheral ^{16}O + Au events, where very few target nucleons are directly involved.

It has been shown [3] that particle yields in the target rapidity region exhibit a proportionality to the target mass. It is therefore of interest to compare proton multiplicities with the measured radius parameters. Such a comparison is displayed in Fig. 8 – here all analyzed systems including the different centrality cuts in the ZDC-energy for the Au-target are shown.

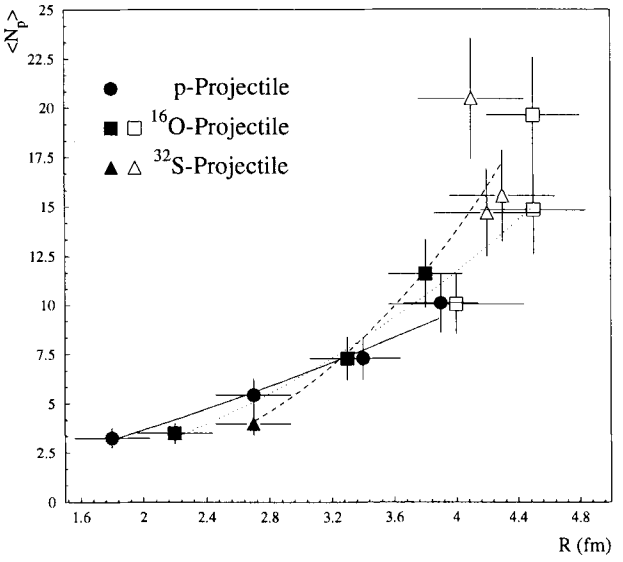

Fig. 8. The average proton multiplicity $< N_p >$ as a funcion of the radius parameters R for all analyzed systems. The open symbols display the values for the Au-target with the different centrality cuts. The results of the different fits as described in the text are represented by the lines. $< N_p >$ is weighted with the number of proton pairs in each event and obtained with the same proton identification window for the proton-, ^{16}O-, and ^{32}S-data, in order to make a direct comparison possible. The values displayed here for $< N_p >$ are efficiency corrected as explained in the text

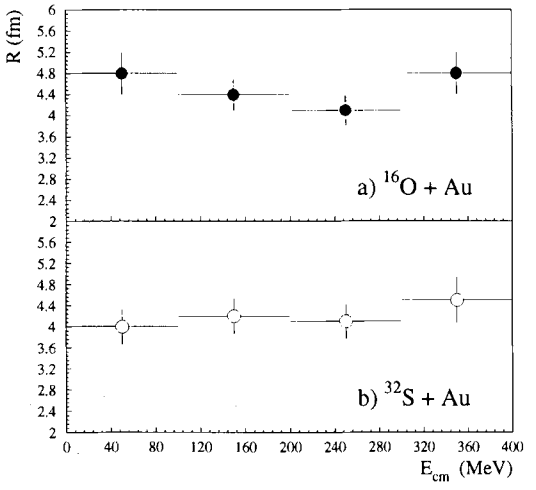

Fig. 9. Radius parameters R for ^{16}O and ^{32}S + Au reactions as a function of the center-of-mass energy E_{cm} of the proton pairs

The observed relation ressembles very much one would expect from the target dependence investigated above: The data for all projectiles show a similar behaviour. When the proton multiplicity is parameterized as a power of the radius, an exponent of $\beta' = 2.1 \pm 0.5$ can be extracted. Despite this overall ressemblance there are differences in the behaviour for different projectiles. Proton induced reactions show a much smaller exponent of $\beta' = 1.4 \pm 0.3$, while the fit yields a power $\beta' = 2.1 \pm 0.7$ for ^{16}O and $\beta' = 3.1 \pm 0.9$ for ^{32}S projectiles.

Figure 9 shows the dependence of the radius parameters on the center-of-mass energy $E_{cm} = \mathbf{P}^2/(4\,m_p)$ of the proton pairs. Systems with a nonzero lifetime could reveal an increase of R with the energy of the proton pairs [7] since the longitudinal expansion of the source is of the order of $(P_{cm}/2\,m_p)\,\tau$. For the systems analyzed here, there is no such effect visible.

4 Discussion

Protons in the target fragmentation region may originate from two mechanisms. They may either participate only in the primary reaction and leave the target nucleus without further interaction, or they may be involved in rescattering processes – as participants or target spectators. These two mechanisms should also be reflected in the respective source sizes for these particles. Primary participant protons originate from the overlap region of projectile and target – their source size should depend on both projectile and target mass. Rescattered participants or spectators may undergo their last interaction anywhere in the target – their source size should exhibit mainly a strong target dependence. The observation that proton source radii are close to the geometric radii of the target and show an approximate proportionality to $A_{\mathrm{Target}}^{1/3}$ illustrates the importance of the rescattering processes.

Protons emitted into the backward hemisphere cannot originate from a single binary nucleon-nucleon collision. They have to undergo rescattering. This is in line with the observation of a stronger target dependence of the radii for angles $\theta_{\mathrm{lab}} > 90°$.

In the forward hemisphere the target dependence is weaker – this can be expected, because here protons from primary reactions may also contribute.

The angular dependence of the radii for the heaviest systems (^{16}O and ^{32}S + Au, see Fig. 6) may be taken as another hint for the existence of these two proton sources. The contribution from the participants reduces the effective source size for forward angles. These heavy systems obviously provide a situation, where both mechanisms are observable. This is not as clear for other systems: light targets do not allow rescattering to be as important. The comparably small radius value at backward angles for the reaction p + Cu, for example would not be expected for a scenario of 'complete rescattering'. The full understanding of these values obviously requires a better knowledge of the space-time development in the target region.

From the comparison of proton yields and radii (Fig. 8) one can see that data for different projectiles exhibit different behaviour. For proton projectiles the increase of proton yields with increasing radii is much weaker than for heavier projectiles. Obviously the number of emitted protons varies for different systems, which could be understood as a different degree of excitation. The uncertainties do not allow to analyze this in more detail, but this example may illustrate that the study of particle yields on its own is not sufficient to understand the reaction geometry.

The observation, that there is no centrality dependence for the Au target, fits into this picture. Even a peripheral collision excites the full target nucleus, but the degree of excitation may vary.

Table 5. Radius parameters R in fm for p and ^{16}O reactions for protons observed in the forward and backward θ_{lab}-angle regions

Projectile	θ_{lab}-Range	Target			
		Au	Ag	Cu	C
p	$< 90°$	3.9 ± 0.24	3.5 ± 0.24	3.0 ± 0.24	1.8 ± 0.34
	$> 90°$	4.0 ± 0.34	3.2 ± 0.24	2.0 ± 0.24	1.5 ± 0.24
^{16}O	$< 90°$	4.2 ± 0.30	3.8 ± 0.24	3.3 ± 0.24	2.3 ± 0.24
	$> 90°$	4.6 ± 0.34	4.0 ± 0.34	3.3 ± 0.24	1.6 ± 0.34

5 Summary and conclusions

We have presented an analysis of two-proton correlations in the target fragmentation region of proton-, ^{16}O-, and ^{32}S-induced reactions with various targets at 200 A GeV. By comparing the correlation function with the results of simulations, it was possible to extract radius parameters.

The proton source is mainly determined by the geometry of the target nucleus. The measured values show a dependence on the target mass similar to $\propto A_{Target}^{1/3}$ and are close to the nuclear radii. The target dependence is stronger for protons than for ^{16}O projectiles. The whole target is involved in the reaction, even in proton induced reactions and also in peripheral heavy ion collisions. This is in agreement with the observation, that the charged particle multiplicity is proportional to the number of target nucleons [3].

The target dependence is stronger in the backward hemisphere $\theta_{lab} > 90°$ than in the forward hemisphere $\theta_{lab} < 90°$, but the difference is less pronounced for the ^{16}O-induced reactions than for the proton reactions.

There is no variation of the radius parameters with the center-of-mass energy E_{cm} of the proton pairs. This indicates, that lifetime effects do not play an important rôle, so that the extracted radius parameters gives a good description of the actual proton source.

It has also been shown that the study of particle yields does not allow a direct conclusion on geometric properties of the reaction. In the target region the number of protons emitted per unit volume changes for different reactions.

Acknowledgements. This work was partially supported by the German BMFT, the United States DOE, the Swedish Natural Science Research Council and the Alexander von Humboldt Foundation. We gratefully acknowledge the contributions of S. Pratt to this analysis, who provided the computer code for the calculation of the correlation function. We also like to thank the accelerator divisions of CERN for their excellent work.

References

1. R. Albrecht et al. (WA80 Collaboration): Z. Phys. C45 (1990) 529
2. R. Albrecht et al. (WA80 Collaboration): Z. Phys. C53 (1992) 225
3. R. Albrecht et al. (WA80 Collaboration): Z. Phys. C55 (1992) 539
4. R. Albrecht et al. (WA80 Collaboration): Z. Phys. C57 (1993) 37
5. R. Albrecht et al. (WA80 Collaboration): Phys. Lett. B307 (1993) 269
6. S. E. Koonin: Phys. Lett. B70 (1977) 43
7. S. Pratt and M. B. Tsang: Phys. Rev. C36 (1987) 2390
8. W. Bauer, C. K. Gelbke and S. Pratt: Ann. Rev. Nucl. Part. Sci. 42 (1992) 77
9. H. Gustafsson et al. (Plastic Ball Collaboration): Phys. Rev. Lett. 53 (1984) 544
10. A. Baden et al.: Nucl. Instr. and Meth. A203 (1982) 189
11. G. R. Young et al.: Nucl. Instr. and Meth. A279 (1989) 503
12. B. Nilsson-Almqvist and E. Stenlund: Comp. Phys. Comm. 43 (1987) 387
13. C. Blume: Diploma thesis, University of Münster, (1993)
14. G. Musiol, J. Ranft, R. Reif and D. Seeliger: Kern- und Elementarteilchenphysik, VCH Verlagsgesellschaft Weinheim (1988)